Thermal evolution of first-order magnetization processes in the single-ion one-sublattice system with uniaxial anisotropy

Ming-hui Yu
Shenyang National Laboratory for Materials Science and International Centre for Materials Physics, Institute of Metal Research, Chinese Academy of Sciences, Wenhua Road 72, Shenyang 110016, People's Republic of China and Van der Waals-Zeeman Instituut, Universiteit van Amsterdam, Valckenierstraat 65 1018 XE Amsterdam, The Netherlands

Zhi-dong Zhang
Shenyang National Laboratory for Materials Science and International Centre for Materials Physics, Institute of Metal Research, Chinese Academy of Sciences, Wenhua Road 72, Shenyang 110016, People's Republic of China

F. R. de Boer, E. Brück, and K. H. J. Buschow
Van der Waals-Zeeman Instituut, Universiteit van Amsterdam, Valckenierstraat 65, 1018 XE Amsterdam, The Netherlands
(Received 22 May 2001; published 13 February 2002)

The thermal evolution of first-order magnetization processes (FOMP's) is intensively studied within a description of the anisotropy energy of a single-ion one-sublattice system with two or three anisotropy constants. By following the temperature-induced trajectories in the anisotropy-parameter plane, all possible types of thermal evolution of the FOMP are detected by an effective parameter method in the mean-field approximation. Within the two-constant approximation, three types of thermal behavior of the FOMP are found. Within the three-constant approximation, 12 types are found when the zero-temperature second-order anisotropy constant K_1^0 is positive, and 14 types when K_1^0 is negative. Phase diagrams for the existence condition of thermal behavior of the FOMP are given in the zero-temperature anisotropy space in combination with analytical and numerical calculations. For each type of variation of the FOMP, an example is selected to describe the temperature dependence of the normalized amplitude and the critical field of the magnetization jump. The relation between the type of variation of the FOMP and the spin-reorientation transition is discussed in detail.

DOI: 10.1103/PhysRevB.65.104414 PACS number(s): 75.10.Dg, 75.30.Gw, 75.30.Kz, 75.40.Mg

I. INTRODUCTION

Ferromagnetic materials may show jumps in magnetization for certain combinations of anisotropy constants.[1] These so-called first-order magnetization processes (FOMP's) have been observed in a large variety of magnetic materials.[2–7] The nature of this phenomenon is the same as that of a discontinuous spin-reorientation transition (SRT), which may be found with changing temperature. A FOMP occurs between two inequivalent minima of free energy that correspond to two particular directions of the magnetization vector **M**, and is an irreversible rotation of the magnetization vector **M** between two inequivalent magnetization states $\mathbf{M}_1$ and $\mathbf{M}_2$ in an external magnetic field. During the FOMP, the moment reorientation must overcome an energy barrier which may be equal to the energy maximum between the two energy minima or to the energy needed for the nucleation and displacement of domain walls, depending on the magnetization mechanism of the jump, e.g., coherent rotation or domain-wall nucleation and displacement. If thermal excitation cannot supply enough energy for the magnetic moment to surpass the energy barrier, hysteresis will be present in the magnetization curve, which is a common feature of first-order transitions. However, it is usually difficult to observe the hysteresis in FOMP's, except perhaps at very low temperatures.[8] This is probably due to the low-energy barrier between the two states or to the very low coercivity which is inherent to this kind of magnetization process.

Asti and Bolzoni[9] carried out a complete phenomenological analysis of FOMP's in uniaxial crystals within a three-constant approximation to the anisotropy energy. Six types of FOMP's ($A1$, $A1C$, $A2$, $P1$, $P1C$, and $P2$) were defined, where A (P) means that the magnetic field is applied parallel (perpendicular) to the c axis. If the final state after the transition is the saturation state, the FOMP is of type 1; otherwise it is of type 2. The letter C denotes that the uniaxial anisotropy is of easy-cone type. Analytical expressions, computed plots, and diagrams of the critical parameters (critical magnetization and critical field) were given in detail in Ref. 9. Asti and Bolzoni gave a unified view of FOMP's in uniaxial crystals, and provided a method for a highly accurate determination of the anisotropy constants at the temperature where the phenomenon is present. Further study of the transformation of the singularity from FOMP's in the case of a polycrystalline uniaxial specimen revealed that for FOMP's of type P a discontinuity appears in the first derivative of the magnetization with respect to the magnetic field and that a FOMP of type A gives rise to a discontinuity in the second derivative.[10] These results lead to an extension of the singular-point-detection theory, with the possibility of measuring the critical field using polycrystalline specimens.

A FOMP can usually be observed only in a restricted temperature range. Thus, another important parameter, the critical temperature, is frequently used to indicate the tempera-

tures for onset and disappearance of a FOMP. Up to now, a systematic and complete study of the thermal behavior of a FOMP has been absent, mainly due to the complexity of the problem. The main difficulties for a theoretical study are how to determine accurately the temperature dependence of the anisotropy constants, and how to understand the effect of temperature on the critical parameters of FOMP's. It is necessary to understand well how the trajectory undergone by the anisotropy constants in the parameter space varies with changing temperature. Recently, a very effective parametric method was successfully applied to the Callen-Shtrikman theory of magnetic single-ion anisotropy by Millev and Fähnle,[11,12] and was shown to be applicable within the frameworks of the mean-field (MF) approximation and the random-phase approximation.[12] This parametric method makes it possible to calculate the exact thermal averages of the Stevens operators[13,14] for arbitrary temperature and for any value of the angular moment J, without any confinement or assumption,[15–17] and only needing to sweep the generalized effective field between zero and infinity.[18–21] Consequently, the temperature dependence of the single-ion anisotropy can be precisely calculated without recourse to iteration.[18,19] In our previous work,[22] the temperature dependence of the uniaxial magnetic anisotropy constants and the SRT in the single-ion one-sublattice system were intensively investigated by means of an effective parametric method. In the present work, taking advantage of the parametric method, we thoroughly study the thermal evolution of a FOMP in the single-ion one-sublattice system by tracing the evolution of the anisotropy flow induced by a temperature variation in the anisotropy space. This provides a clear insight into the unusual magnetization processes occurring in ferromagnetic uniaxial crystals.

The remainder of the present paper is organized as follows. The theoretical outline of the calculation method will be described briefly in Sec. II. Section III is devoted to analyzing the thermal evolution of a FOMP in a single-ion one-sublattice system. As a starting point, in Sec. III A, we first deal with the simple case of a description of the anisotropy energy in terms of two anisotropy constants. The much more complicated case of three anisotropy constants will be presented in Sec. III B. A summary is given in Sec. IV.

II. THEORETICAL OUTLINE

A one-sublattice system with uniaxial anisotropy in an external magnetic field can be described phenomenologically by the free energy, involving the magnetocrystalline anisotropy energy and the magnetostatic energy:

$$F = K_1 \sin^2\theta + K_2 \sin^4\theta + K_3 \sin^6\theta - HM_s \cos(\theta-\varphi), \quad (1)$$

where K_1, K_2, and K_3 are the uniaxial anisotropy constants. The in-plane anisotropy is assumed to be negligible. θ and φ are the angles of the magnetization vector **M** and the applied magnetic field **H** with respect to the symmetry axis c, respectively. The magnetization processes always take place in the (c, **H**, **M**) plane, since the in-plane contributions to anisotropy are neglected in Eq. (1). If the direction of the magnetic field is fixed, the magnetization curve is determined by a stable moment configuration corresponding to the absolute minimum of the free energy. The absolute minimum of the free energy can be found by minimizing Eq. (1) with respect to the angle θ, which involves the first and second partial derivatives of the free energy with respect to the angle θ:

$$\frac{\partial F}{\partial \theta} = \sin 2\theta(K_1 + 2K_2 \sin^2\theta + 3K_3 \sin^4\theta) + HM_s \sin(\theta-\varphi) = 0, \quad (2)$$

$$\frac{\partial^2 F}{\partial \theta^2} = 2K_1 - 4(K_1 - 3K_2)\sin^2\theta - 2(8K_2 - 15K_3)\sin^4\theta - 36K_3 \sin^6\theta + HM_s \cos(\theta-\varphi) > 0. \quad (3)$$

The solutions satisfying Eqs. (2) and (3) correspond to the local energy minima, among which the absolute minimum is chosen to determine the equilibrium state. If two absolute minima coexist, a discontinuous jump of the magnetization is expected to occur. By considering the condition of two coexisting minima, Asti and Bolzoni[9] made a detailed study of the magnetic phase diagrams of FOMP's for two cases: the applied field **H** either parallel or perpendicular to the c axis (type-A and type-P FOMP's, respectively). The borderlines between the six types of FOMP's ($A1$, $A1C$, $A2$, $P1$, $P1C$, and $P2$) were analytically derived. The critical field and magnetization were determined so that the type of FOMP and the location and the amplitude of the jump can be predicted if one knows the values of the anisotropy constants.

In order to determine the thermal evolution of a FOMP, one needs to know the temperature dependence of the anisotropy constants. The theoretical framework of the parametric method for the temperature dependence of the anisotropy constants was described in detail in Ref. 22. Here we shall introduce this briefly for the convenience of the reader. In a single-ion one-sublattice system, the temperature dependence of the anisotropy constants can be determined through its relations to the theoretically more fundamental anisotropy coefficients $\overline{\kappa_n}$ [see Eqs. (A1)–(A3) in Appendix (A)].[1,22,23] The zero-temperature (ground-state) anisotropy constants are $K_i^0 \equiv K_i(T=0)$. The anisotropy coefficients are associated with the thermal averages of the Stevens operators $\langle \hat{O}_n^0 \rangle (T)$ normalized to their zero-temperature values.[11,22,24,25] In the case that the exchange interaction is dominant, i.e., if the crystal-field anisotropy terms are much smaller than the quantum-mechanical exchange, which is usually represented by a Heisenberg-exchange term in the Hamiltonian which is responsible for the strong magnetic behavior of the system of interacting moments,[24,26] based on first-order thermodynamic perturbation theory the anisotropy coefficients turn out to be linear combinations of the moments $M_n \equiv \langle (\hat{J}_z)^n \rangle$ [see Eqs. (A4)–(A6) in Appendix A]. Here $\hat{J}_z$ is the z component of the angular momentum operator of a given ion; $p_n(J) \equiv \langle \hat{O}_n^0 \rangle (0)$ are certain J-dependent products.[14] All the moments M_n and, consequently, all $\overline{\kappa_n}$'s, can be expressed via the first moment M_1 or, equivalently, the reduced magnetization $m = M_1/J$. The functional dependence $M_n = M_n(M_1)$ itself proves to be model independent in all renormalized quasi-independent collective-excitation theo-

ries. All the moments M_n can be easily derived from the moment-generating function $\Omega(\alpha,x)$ by means of nth-order partial derivatives with respect to α [see Eq. (A7) in Appendix A]. In the MF and dominant-exchange approximations, neglecting the influence of an applied magnetic field on the magnetic order, one can derive a simple expression for the relation between x and t [$t \equiv T/T_c$ and T_c is the MF Curie temperature; see Eq. (A8) in Appendix A]. Therefore, the temperature dependence of the anisotropy coefficients and anisotropy constants for any J can be indirectly computed in the whole ordering temperature range by using the generalized effective field x as a parameter.[20,22] By means of this effective parametric method, a general discussion and classification of the temperature dependence of the uniaxial anisotropy constants was exhaustively performed in Ref. 22 for a single-ion one-sublattice system. Subsequently, all possible SRT's were detected by tracing the evolution of the anisotropy flow in the anisotropy space including the phase diagrams for easy-magnetization directions (EMD's).

In the present contribution, the thermal evolution of a FOMP in a single-ion one-sublattice system will also be thoroughly investigated by tracing the evolution of the anisotropy flow in the anisotropy space, but involving the phase diagrams for the existence of the FOMP.

III. TYPES OF THERMAL EVOLUTION OF FOMP'S

The anisotropy coefficients $\overline{\kappa_n}$ are the basis functions that describe the temperature dependence of the anisotropy constants. The temperature dependence of the anisotropy coefficients is uniquely determined by a given J.[12,20,22] For any value of J, all three basis functions decrease strictly monotonically with increasing temperature. $\overline{\kappa_2}$ is convex upward in the whole temperature range, while both $\overline{\kappa_4}$ and $\overline{\kappa_6}$ possess a typical bell shape and an inflection point.[12,22] An exception to the convex-upward behavior of $\overline{\kappa_2}$ is its strictly linear behavior in the classical limit of $J \to \infty$. The higher the order of the anisotropy coefficient, the faster it decreases with increasing temperature. Provided J is fixed, the temperature dependence of the anisotropy constants is solely determined by the set of zero-temperature anisotropy constants K_1^0, K_2^0, and K_3^0 [see Eqs. (A1)–(A3) in Appendix A]. Since a variation of J does not affect the general classification of the types of anisotropy constants, $J=3$ is usually chosen in the calculation procedure.[19,22] This will make neither the analysis nor its exposition longer. As long as the zero-temperature constants are known, the exact temperature dependence of the anisotropy constants can be accurately calculated by the above-mentioned parametric method within the mean-field approximation. Subsequently, the temperature-driven anisotropy flow can be depicted through the trajectory followed by the anisotropy constants in anisotropy space when the temperature is varied.[20] If this trajectory crosses the borderline separating different regions of stable magnetic phases, a magnetic phase transition is expected at the crossing point.[22] If the phases have different EMD's, an SRT will take place. If the phases have different FOMP's, the type of FOMP will change. In a one-sublattice system, the competition between different anisotropy constants is responsible for the occurrence of a SRT, while the competition between the anisotropy energies and the magnetostatic energy is responsible for the occurrence of a FOMP. However, the thermal behavior of a FOMP in a one-sublattice system is attributed to the competition between the different anisotropy constants. Thus it would be possible to investigate the thermal evolution of a FOMP in a one-sublattice system by observing the thermal behavior of the anisotropy constants, analogously to the way we have previously carried out a systematic analysis of a SRT.[22]

A. Case of two anisotropy constants

If the highest-order zero-temperature anisotropy constant is zero ($K_3^0=0$), only two constants are required to describe the uniaxial anisotropy. In this case, as shown in Eq. (A2) in Appendix A, K_2 has the same temperature dependence as the fourth-order anisotropy coefficient. Consequently, $K_2(t)$ decreases (or increases) strictly monotonically for $K_2^0>0$ (or $K_2^0<0$) with increasing temperature. As to K_1, both second- and fourth-order basis functions enter into its expression, so that three generic types of variation of $K_1(t)$ exist, that depend only on the ratio $x_0=K_2^0/K_1^0$ of the zero-temperature anisotropy constants: (i) for $x_0>\frac{3}{8}$, $K_1(t)$ has an extremum that is a minimum or a maximum depending on the sign of K_1^0; (ii) for $-\frac{7}{8}<x_0<\frac{3}{8}$, $K_1(t)$ decreases (or increases) strictly monotonically for $K_1^0>0$ (or $K_1^0<0$); and (iii) for $x_0<-\frac{7}{8}$, $K_1(t)$ has a zero point at a certain temperature between zero Kelvin and Curie temperatures.[20] Since the temperature dependence of K_1 and K_2 is solely determined by the zero-temperature conditions, i.e., the values of K_1^0 and K_2^0, these values are of crucial importance. If the pair of K_1^0 and K_2^0 is given, the temperature flow of the anisotropy is fully determined within the MF approximation, and is valid for the whole class of nontrivial collective-excitation theories.[24] Illustrative results are shown in Fig. 1 for all typical initial conditions and theoretical trajectories are presented for the anisotropy in the three generic regimes discussed above. As the anisotropy constant K_2 evolves upon variation of temperature without changing its sign, a trajectory starting in the upper ($K_2>0$) or lower ($K_2<0$) half-plane will stay in its plane. If the anisotropy constant K_1 has a zero point, a flow starting in the right ($K_1>0$) or left ($K_1<0$) half-plane will leave its plane (i.e., will cross the borderline of the two half-planes) at the temperature where K_1 changes its sign. At $t=1$, all trajectories flow into the origin with a slope approaching zero, because both single-ion anisotropy constants become zero at the Curie temperature and K_2 decreases faster than K_1 at high temperatures.[24,27] The thick solid lines in Fig. 1 are the borderlines for the existence of $A1$ and $P1$ FOMP's. This picture is static in the sense that at a given temperature, say, T_1, $K_1(T_1)$ and $K_2(T_1)$ have definite values that determine a point in the K_1-K_2 plane, and variations of the temperature and applied magnetic field do not affect the location of the borderlines. After scrutinizing the anisotropy trajectories in the case of two anisotropy constants, as shown in Fig. 1, three kinds of crossovers exist between the trajectories and the borderlines. Accordingly, three types of thermal evolutions of the FOMP's take place: (i) $P1$, (ii)

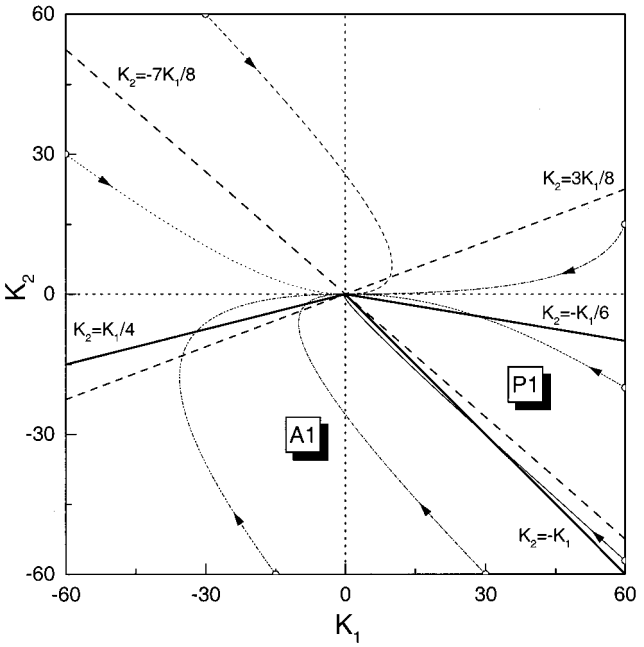

FIG. 1. Anisotropy flow diagram in the $(K_1$-$K_2)$ plane. The solid lines are the borderlines between the $A1$ and $P1$ types of FOMP's. The dashed straight lines represent the results of the analysis of the types of temperature dependence of K_1 within the two-constant approximation. The representative initial conditions $(K_1^0-K_2^0)$ can be read off the coordinates of the open circles. The arrows indicate the direction of temperature evolution as T increases from zero to T_C.

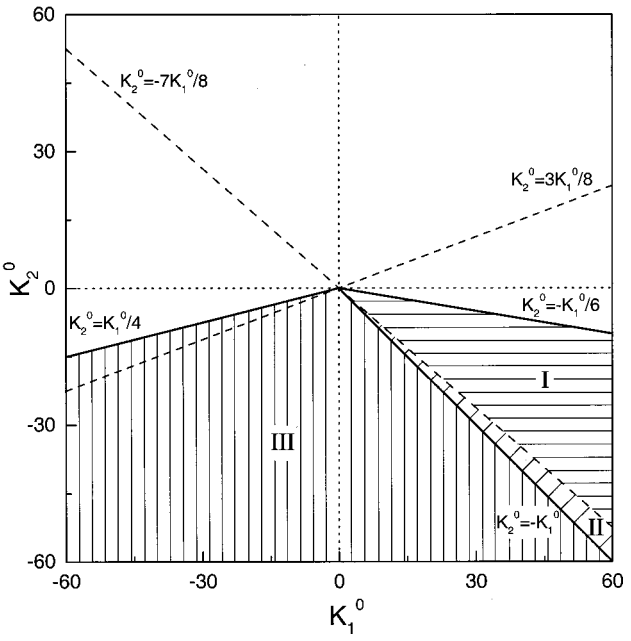

FIG. 2. Phase diagram in the $(K_1^0$-$K_2^0)$ plane for different kinds of thermal behaviors of the FOMP's: (*I*) $P1$, (*II*) $P1$-$A1$, (*III*) $A1$.

$P1$-$A1$, and (iii) $A1$. The crossovers are unique, and take place at a certain critical temperature T_{cr} corresponding to the disappearance or a change of the type of FOMP. The existence and type of the crossovers are determined solely by the zero-temperature values of K_1^0 and K_2^0. As shown in Fig. 2, at zero temperature, three hatched areas *I*, *II*, and *III* can be distinguished in the K_1^0-K_2^0 plane, that correspond to the three types of the crossovers. All three areas are in the lower half-plane. That is, $K_2^0<0$ is a prerequisite for the existence of a FOMP in the case of two anisotropy constants. The areas are defined as follows:

$$(I)\ \text{the } P1 \text{ area:} \quad -\tfrac{7}{8}K_1^0<K_2^0<-\tfrac{1}{6}K_1^0, \quad K_1^0>0,$$

$$(II)\ \text{the } P1\text{-}A1 \text{ area:} \quad -K_1^0<K_2^0<-\tfrac{7}{8}K_1^0, \quad K_1^0>0,$$

$$(III)\ \text{the } A1 \text{ area:} \quad 4K_2^0<K_1^0<-K_2^0, \quad K_2^0<0.$$

The conditions listed above are for the existence of the three types of the thermal behavior of the FOMP. The borderlines for the disappearance of the FOMP's of type $A1$ and $P1$ are $K_2^0=\frac{1}{4}K_1^0$ and $-\frac{1}{6}K_1^0$, respectively. The crossover from $P1$ to $A1$ is at $K_2^0=-K_1^0$. It is interesting to note that the $P1$-$A1$ area is the same as the axis (A) to plane (P) wedge in Fig. 3 of Ref. 20, which means that all systems in this area possess both a SRT from A to P, and a change of FOMP type from $P1$ to $A1$.

As to the critical temperature T_{cr} of the FOMP, the K_2 vs K_1 plots are only indicative. However, it is easy to determine the critical temperature, if one plots the ratio $\rho(t)=K_1(t)/K_2(t)$ as a function of the reduced temperature t. In Fig. 3, we present $\rho(t)$ for some representative cases for which a crossover is detected. From the intersections of $\rho(t)$ with the lines of crossover $\rho_{cross}=4$, -1, and -6, one is able to determine T_{cr} unambiguously for the corresponding crossover. When the crossovers take place with increasing the temperature, the FOMP will disappear or its type will

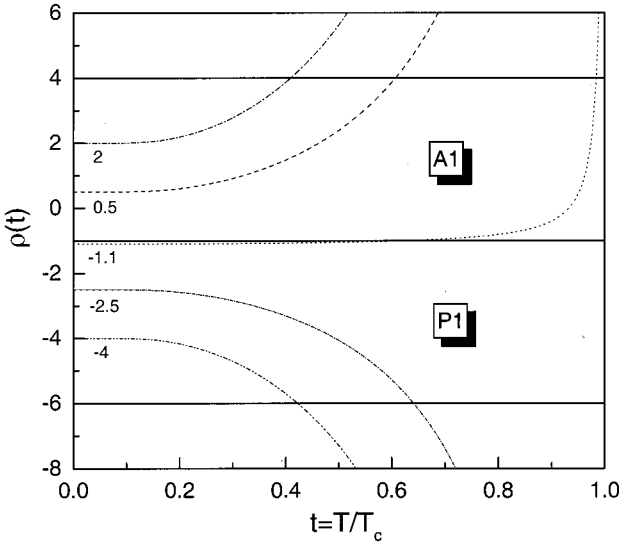

FIG. 3. Temperature dependence of the ratio of the first and second anisotropy constants $\rho(t)=K_1(t)/K_2(t)$. The solid horizontal lines $\rho_{cross}=4$, -1, -6 are the borderlines between the $A1$ and $P1$ types of FOMP's in the representation $\rho=\rho(t)$; crossing these lines corresponds to disappearance or to type changes of the FOMP's.

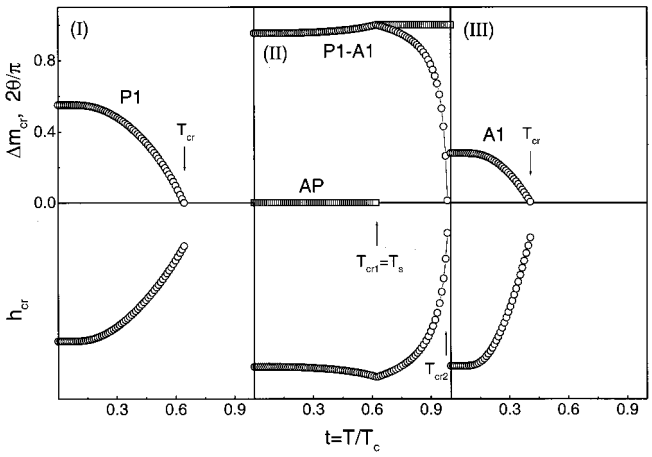

FIG. 4. Temperature variation of the angle of the EMD with respect to the *c* axis, normalized to $\pi/2$ (open squares), the normalized amplitude, and the critical field of the FOMP's (open circles) in some typical systems. The initial ratios between the first and second anisotropy constants used in the calculation are (*I*) -2.5, (*II*) 1.1, and (*III*) 2.0.

change. Usually, one is interested in the critical field and the amplitude of a FOMP; thus it is meaningful to study the thermal behavior of the critical field and the amplitude before the jump disappears. As shown in Ref. 9, one easily obtains an expression in terms of $x=K_2/K_1$ for the normalized critical field $h_{cr}=H_{cr}/|H_a|$ (where H_a is the anisotropy field), the normalized amplitude $\Delta m_{cr}=\Delta M_{cr}/M_s$ (where M_s is the saturation magnetization), and the normalized critical magnetization $m_{cr}=M_{cr}/M_s$ (where M_{cr} is the magnetization at the initial state of the FOMP). For a $P1$ type of FOMP, one obtains, using $H_a=2K_1/M_s$,

$$m_{cr}=\frac{\sqrt{-2-3/x}-1}{3}, \tag{4}$$

$$\Delta m_{cr}=1-m_{cr}, \tag{5}$$

$$h_{cr}=m_{cr}(1+2xm_{cr}^2). \tag{6}$$

For an $A1$ type of FOMP with $H_a=[-2(K_1+2K_2)]/M_s$, one obtain

$$m_{cr}=\frac{\sqrt{4+3/x}-1}{3}, \tag{7}$$

$$\Delta m_{cr}=1-m_{cr}, \tag{8}$$

$$h_{cr}=\left|\frac{m_{cr}[1+2x(1-m_{cr}^2)]}{1+2x}\right|. \tag{9}$$

The temperature dependence of the normalized amplitude and the critical field are shown in Fig. 4 for three typical cases, corresponding to three kinds of thermal evolution of the FOMP. In the cases of $P1$ and $A1$, the normalized amplitude decreases to zero if the temperature increases from zero to the critical temperature, whereas the normalized critical field increases to a maximum. In the case of $P1$-$A1$, the first critical temperature T_{cr1} is equal to the axis-to-plane SRT temperature T_s. This shows that the change of the type of FOMP is due to the change of the EMD from axis to plane (see the angle of the EMD with respect to the *c* axis) at the first critical temperature. Below T_{cr1}, the normalized amplitude increases to unity and the normalized critical field decreases to zero with increasing temperature. Then the normalized amplitude decreases to zero, and the normalized critical field increases to a maximum, as the temperature increases from T_{cr1} to T_{cr2}. Above T_{cr2}, no FOMP is observed, and the EMD remains in the plane. Therefore, in the case of two anisotropy constants, one-sublattice systems with zero-temperature anisotropy constants in area *II* are rich of magnetic phenomena, like a first-order axis-to-plane *AP* SRT, a $P1$ type of FOMP at low temperatures ($T<T_{cr1}$) and an $A1$ type of FOMP at high temperatures ($T_{cr1}<T<T_{cr2}$).

B. Case of three anisotropy constants

If the zero-temperature highest-order anisotropy constant is nonzero ($K_3^0\neq 0$), three constants are needed to describe the uniaxial anisotropy. In this case, the third anisotropy constant has the same temperature dependence as the sixth-order anisotropy coefficient. Just like K_1 in the case of two anisotropy constants, in the case of three anisotropy constants K_2 possesses three generic types of thermal behavior depending on the ratio of the intrinsic constants $r=K_3^0/K_2^0$, because the fourth- and sixth-order basis functions enter into the expression for the temperature dependence. If $r>\frac{5}{9}$, $K_2(t)$ has an extreme value. For $-\frac{11}{18}<r<\frac{5}{9}$, $K_2(t)$ is a strictly monotonic function. If $r<-\frac{11}{18}$, $K_2(t)$ becomes zero at some temperature.[22] In the three-constant case, the temperature dependence of K_1 becomes very complicated due to the three basis functions and two independent variables $x_0=K_2^0/K_1^0$ and $y_0=K_3^0/K_1^0$ involved in Eq. (A1). As a result of all possible combinations between x_0 and y_0, seven types of temperature dependence of $K_1(t)$ may be observed. A detailed phase diagram for these different temperature dependencies in the parameter space (x_0-y_0) was presented in Fig. 4 of Ref. 22. The most interesting feature is that, in the case of the seventh type, $K_1(t)$ may exhibit two zero points, i.e., it changes sign twice for realistic values of the initial parameters. This results in a trajectory that is cut into three parts distributed over the two parameter spaces (x-y) with $K_1(t)>0$ and $K_1(t)<0$,[21] that are needed for a complete description of the anisotropy in the case of three constants.[9] Here $x=K_2/K_1$ and $y=K_3/K_1$. When $K_1(t)$ goes to zero, the trajectory comprising the points $[x(t),y(t)]$ will go to infinity in the chosen parameter space and, after the change of sign of $K_1(t)$, re-emerge in another section of the parameter space. If $K_1(t)$ has only one zero point, its trajectory will consist of two parts. If $K_1(t)$ has no zero point, it will not leave the parameter space determined by the sign of K_1^0. Generally speaking, the trajectory $[x(t),y(t)]$ starts from the initial point (x_0,y_0), and finally ends in the origin, at the Curie temperature, except for some special cases.[22]

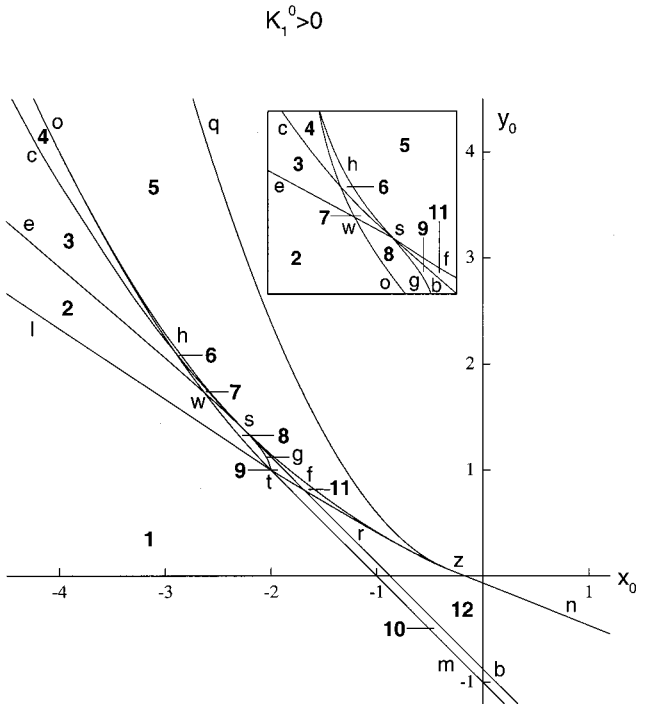

FIG. 5. Phase diagram for different kinds of thermal behavior of the FOMP's in the initial parameter space (x_0-y_0) with $K_1^0>0$: (1) $A1$, (2) $A1C$-$A1$, (3) $A1C$, (4) $A1C$-$P2$, (5) $P2$, (6) $P2$-$A1C$-$P2$, (7) $P2$-$A1C$, (8) $P2$-$A1C$-$A1$, (9) $P2$-$P1$-$A1$, (10) $P1$-$A1$, (11) $P2$-$P1$, and (12) $P1$. The curves *q*, *o* and *r* and the straight lines *l*, *m*, and *n* are the borderlines between four types of FOMP's: $A1$, $A1C$, $P1$, and $P2$ at zero temperature. The configurations of different regions around point *w* are schematically represented in the inset.

1. $K_1^0>0$

In the case of $K_1^0>0$, 12 types of thermal behavior of a FOMP are found after detailed investigation of the trajectories for all possible initial points (x_0,y_0): (1) $A1$, (2) $A1C$-$A1$, (3) $A1C$, (4) $A1C$-$P2$, (5) $P2$, (6) $P2$-$A1C$-$P2$, (7) $P2$-$A1C$, (8) $P2$-$A1C$-$A1$, (9) $P2$-$P1$-$A1$, (10) $P1$-$A1$, (11) $P2$-$P1$, and (12) $P1$. The phase diagram is summarized in Fig. 5, where lines *l*, *m*, and *n* and curves *q*, *o*, and *r* are the borderlines between four types of FOMP's $A1$, $A1C$, $P1$, and $P2$ at zero temperature. The equations of the borderlines in Fig. 5 are listed in Appendix B. Line *b* starts at point $s(-9/4,11/8)$, which is a common intersection point of curves *c*, *e*, *g*, *f*, and *h*. At point *s*, all three anisotropy constants possess the same temperature dependence as the third anisotropy coefficient, so that the trajectory will always be at this point with varying temperature. Point *s* is the crossing point for four types of thermal behavior of K_1, which makes it an important point in the phase diagram.[22] Twelve typical initial points are chosen to represent the 12 types of thermal behavior of the FOMP. Each initial point is symbolized by a letter between *a* and *l*, where *a* corresponds to the initial point in region 1, *b* to that in region 2, etc. For all initial points, the thermal variation of the normalized amplitude and critical field of the FOMP, and the normalized angle of the EMD with respect to the *c* axis (if an SRT exists) are displayed in Figs. 6–9. Furthermore, the relevant anisotropy flows are drawn all together in the *x*-*y* planes in Fig. 10 and labeled with the same letters. In Fig. 10, the dotted curves *o*, *o'*, *p*, *q*, *q'*, *r*, and *r'* and the dotted lines *l*, *m*, *n*, and *n'* denote the borderlines between the six types of FOMP's: $A1$, $A1C$, $A2$, $P1$, $P1C$, and $P2$, at arbitrary temperature. The equations of borderlines in Fig. 10 are listed in Appendix C.

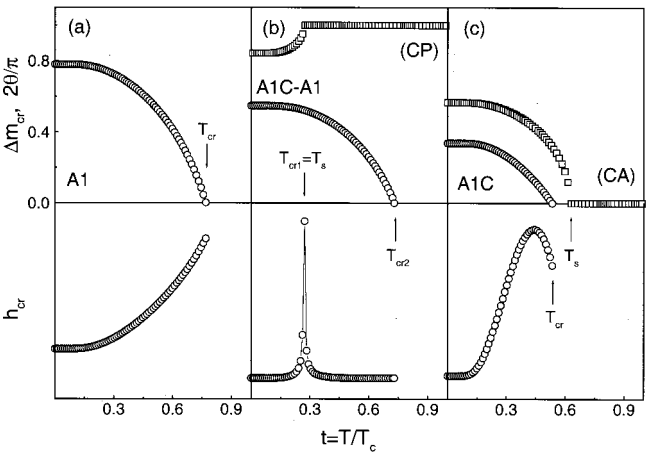

FIG. 6. Temperature variation of the angle of the EMD with respect to the *c* axis, normalized to $\pi/2$ (open squares), the normalized amplitude, and the critical field of the FOMP's (open circles) in some typical systems in the case of $K_1^0>0$. The initial parameters used in the calculation are (*a*) $(-3.0,-2.0)$, (*b*) $(-3.0,1.75)$, and (*c*) $(-4.0,3.5)$.

$A1$. Region 1 in Fig. 5, below the lines *l* and *m*, is the largest one. Only an $A1$ type of FOMP is observed in the systems, with initial points inside this regime. The normalized critical parameters m_{cr}, Δm_{cr}, and h_{cr} for an $A1$ type of FOMP in the three-constant case can be determined with the definition of $H_a=[-2(K_1+2K_2+3K_3)]/M_s$,[9] by means of the following equations:

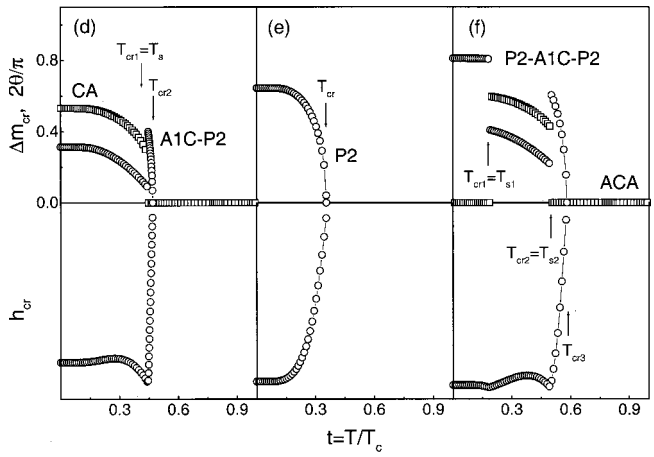

FIG. 7. Temperature variation of the angle of the EMD with respect to the *c* axis normalized to $\pi/2$ (open squares), the normalized amplitude, and the critical field of FOMP's (open circles) in some typical systems in the case of $K_1^0>0$. The initial parameters used during the calculation are (*d*) $(-4.0,3.75)$, (*e*) $(-3.8,4.0)$, and (*f*) $(-3.0,2.262)$.

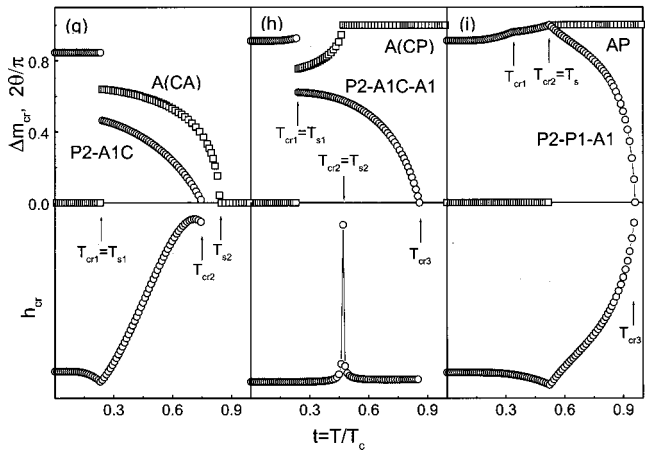

FIG. 8. Temperature variation of the angle of the EMD with respect to the c axis normalized to $\pi/2$ (open squares), the normalized amplitude, and the critical field of FOMP's (open circles) in some typical systems in the case of $K_1^0>0$. The initial parameters used during the calculation are (g) (-2.7,1.85), (h) (-2.3,1.35), and (i) (-1.9,1.0).

$$5ym_{\rm cr}^4+4ym_{\rm cr}^3-3(x+2y)m_{\rm cr}^2-2(x+2y)m_{\rm cr}+x+y+1=0, \tag{10}$$

$$\Delta m_{\rm cr}=1-m_{\rm cr}, \tag{11}$$

$$h_{\rm cr}=\left|\frac{m_{\rm cr}[1+2x(1-m_{\rm cr}^2)+3y(1-m_{\rm cr}^2)^2]}{1+2x+3y}\right|. \tag{12}$$

Figure 6(a) shows the temperature dependence of the normalized amplitude and critical field of an $A1$ type of FOMP below its critical temperature for one typical initial point in this region. Its anisotropy flow a in Fig. 10 contains two parts ($a1$ and $a2$) due to the one zero point of K_1. Below the critical temperature, the normalized amplitude decreases to zero, and the normalized critical field increases to a maximum with increasing temperature. Even if there is a zero point for K_1 below $T_{\rm cr}$, no anomaly occurs in the temperature dependence of $\Delta m_{\rm cr}$ and $h_{\rm cr}$. The disappearance of the $A1$ type of FOMP is due to the crossing of the second part ($a2$) of the anisotropy flow with the borderline n' in the parameter space with $K_1<0$. At the borderline n', the normalized critical amplitude of the jump in the $A1$ type and $A1C$ type of FOMP's is zero.

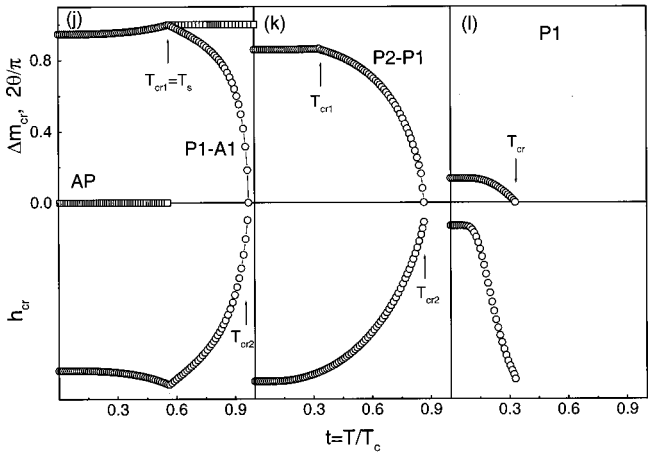

FIG. 9. Temperature variation of the angle of the EMD with respect to the c axis normalized to $\pi/2$ (open squares), the normalized amplitude, and the critical field of FOMP's (open circles) in some typical systems in the case of $K_1^0>0$. The initial parameters used during the calculation are (j) (-1.7,0.8), (k) (-1.75,0.9), and (l) (5.0,-2.5).

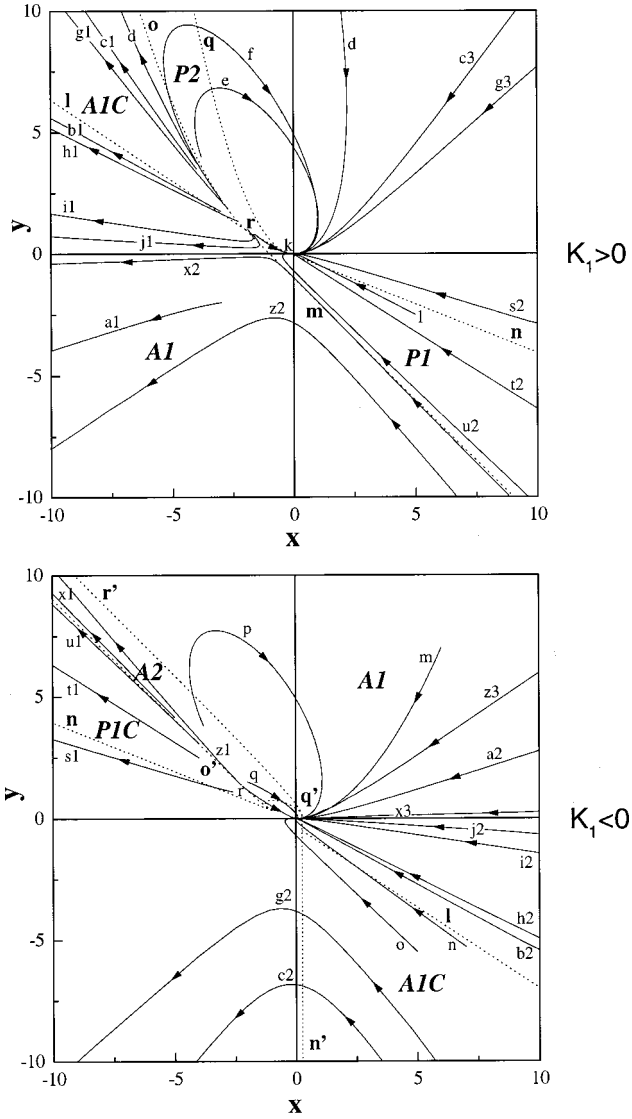

FIG. 10. Anisotropy flows in the plane (x-y) for these typical thermal behaviors of the FOMP's shown in Figs. 6–9 and 12–16. Dotted lines l, m, n, and n' and dotted curves o, o', p, q, q', r, and r' are the borderlines among the six types of FOMP's: $A1$, $A1C$, $A2$, $P1$, $P1C$, and $P2$ at arbitrary temperature. The upper plane corresponds to $K_1>0$, and the lower one to $K_1<0$. The arrows indicate the direction of temperature evolution as T increases from zero to T_c.

$A1C$-$A1$. Region 2 is below curves e and o and above line l in Fig. 5. The systems with initial points inside this area exhibit a continuous cone-to-plane (CP) SRT and two types of FOMP's (an $A1C$ type at low temperature and an

$A1$ type at high temperature). Equations (10)–(12) are also applicable to the $A1C$ type of FOMP. As shown in Fig. 6(b), it is clear that the first critical temperature is equal to the temperature T_s of the (CP) SRT. No anomaly is observed in the temperature dependence of $\Delta m_{\rm cr}$ when the type of FOMP changes from $A1C$ to $A1$. However, $h_{\rm cr}$ has a sharp peak at the first critical temperature. Tracing down the anisotropy flow $b1$-$b2$ in Fig. 10, one finds that its crossing with borderline l is responsible for the (CP) SRT and the FOMP-type variation from $A1C$ to $A1$. The second critical temperature corresponds to the crossing with the borderline n'. At the borderline l, $h_{\rm cr}$ becomes infinitely large, which is the reason why a sharp peak exists in the thermal curve of $h_{\rm cr}$ at the first critical temperature. Curve e in Fig. 5 is numerically determined by collecting the initial points whose trajectories pass through the common crossing point $(\frac{1}{4}, -\frac{1}{2})$ of borderlines l and n' in Fig. 10. If one takes Zener's power law[15] to approximate the temperature dependence of the basis functions $\overline{\kappa_n}$, the equation satisfied by curve e can be deduced [see Eq. (B12) in Appendix B]. When the phase transition takes place at low temperature, Zener's power law will be an easy and effective way to analyze the thermal behavior of the anisotropy.

$A1C$. In region 3 in Fig. 5, below curves c and o and above curve e, the systems possess only an $A1C$ type of FOMP. Curve c is the boundary between the types 4 and 7 of temperature dependence of $K_1(t)$.[22] Line b separates region 3 into two subregions. In the region below line b, $K_1(t)$ has one zero point and a continuous cone-to-plane (CP) SRT can be observed (this case is not illustrated in Fig. 6). In the region above line b, $K_1(t)$ has two zero points and a continuous cone-to-axis (CA) SRT exists [see Fig. 6(c)]. Below the SRT temperature for (CP) or (CA), the $A1C$ FOMP arrives at its critical temperature $T_{\rm cr}$ when the anisotropy flow crosses the borderline n' (see the anisotropy flow $c1$-$c2$-$c3$ in Fig. 10). Above the critical temperature, if the anisotropy flow crosses directly the borderline l, (CP) SRT takes place. If $K_1(t)$ changes its sign twice, (CA) SRT occurs at the second zero point of $K_1(t)$. In the temperature dependence of $h_{\rm cr}$ in Fig. 6(c), there is an extremum below the critical temperature $T_{\rm cr}$, which is due to the large curvature of its anisotropy flow before crossing the borderline n'. When the initial point is just on the line b, no SRT can be observed because the anisotropy flow does not approach the origin but the point $(-\frac{7}{8}, 0)$ in the parameter space with $K_1<0$.

$A1C$-$P2$. Region 4 is above curve c and below curve o. If the anisotropy flow originates from this region [see Fig. 7(d), and the anisotropy flow d in Fig. 10], it first crosses the borderline o, which leads to a discontinuous cone-to-axis CA SRT and simultaneously to a type variation of the FOMP from $A1C$ to $P2$. The critical temperature $T_{\rm cr2}$ for the FOMP of type $P2$ is reached if borderline q is crossed. The normalized critical parameters $\Delta m_{\rm cr}$ and $h_{\rm cr}$ for a $P2$ type of FOMP in the three-constant case can be determined by the following equations with the definition $H_a=2K_1/M_s$ (see Ref. 9),

$$\Delta m_{\rm cr}=\left[\frac{-5x-(60y-11x^2)^{1/2}}{6y}\right]^{1/2}, \tag{13}$$

$$h_{\rm cr}=\frac{A}{5}\left[2-\frac{17x^2+x(60y-11x^2)^{1/2}}{30y}\right], \tag{14}$$

with

$$A=\left[\frac{(60y-11x^2)^{1/2}}{10y}-3x\right]^{1/2}.$$

At $T_{\rm cr1}$, $\Delta m_{\rm cr}$ is discontinuous and $h_{\rm cr}$ becomes zero when the type of FOMP changes from $A1C$ to $P2$. Then, $\Delta m_{\rm cr}$ decreases while $h_{\rm cr}$ increases, until a FOMP of $P2$ type disappears at $T_{\rm cr2}$.

$P2$. Region 5 in Fig. 5 is below curve q and above curves o, h, and f. The systems with the initial points inside this region exhibit only a $P2$ type of FOMP. From the anisotropy flow e in Fig. 10, the disappearance of the $P2$ type of FOMP is due to the crossing of the anisotropy flow with the borderline q. In Fig. 7(e) it is seen that $\Delta m_{\rm cr}$ decreases to zero and $h_{\rm cr}$ increases to a maximum value when the temperature increases to $T_{\rm cr}$. Curve f in Fig. 5 is determined from the initial points whose anisotropy flows pass through the common crossing point z $(-\frac{1}{3}, \frac{1}{15})$ of borderlines q and n. Within the framework of Zener's power law, one can obtain its equation [see Eq. (B13) in Appendix B]. Curve h consists of initial points whose anisotropy flows are tangent with the borderline o.

$P2$-$A1C$-$P2$. Region 6 is enclosed by curves o, c, and h. In systems with initial points inside this region, discontinuous axis-to-cone and discontinuous cone-to-axis ACA SRT and FOMP-type changes $P2$-$A1C$-$P2$ [see Fig. 7(f)] take place. A $P2$-type FOMP can occur when the EMD is an easy axis, both at low temperatures and at high temperatures. The anisotropy flow f shown in Fig. 10 demonstrates that the two crossings with borderline o are responsible for the ACA SRT and the $P2$-$A1C$-$P2$ type change of the FOMP. The crossing with borderline q corresponds to the third critical temperature $T_{\rm cr3}$ at which $\Delta m_{\rm cr}$ of the $P2$ type of FOMP becomes zero. In Fig. 7(f) it is seen that $\Delta m_{\rm cr}$ jumps discontinuously at $T_{\rm cr1}$ $(=T_{s1})$ and at $T_{\rm cr2}$ $(=T_{s2})$.

$P2$-$A1C$. Region 7 is enclosed by curves c, o, and e. Line b separates this region into two subregions. In the region below line b, a discontinuous axis-to-cone and a continuous cone-to-plane $A(CP)$ SRT can be observed, while in the region above line b, a discontinuous axis-to-cone and a continuous cone-to-axis $A(CA)$ SRT exist [see Fig. 8(g)]. When the initial point is just on line b, only a discontinuous axis-to-cone AC SRT is realized. The discontinuous SRT from axis to cone is related to the crossing of the anisotropy flow with borderline o (see the anisotropy flow $g1$-$g2$-$g3$ in Fig. 10). At the same time, the type of FOMP changes from $P2$ to $A1C$ at $T_{\rm cr1}$. Subsequently, when the anisotropy flow crosses the borderline n', the $A1C$ type of FOMP will disappear at $T_{\rm cr2}$. Above $T_{\rm cr2}$, if the anisotropy flow crosses the borderline l, the continuous cone-to-plane SRT will take

place; if $K_1(t)$ has its second zero point, the continuous cone-to-axis SRT occurs [see Fig. 8(g)]; if the anisotropy flow approaches the point $(-\frac{7}{8},0)$, no other SRT is observed. The last case corresponds to the initial points on line *b*.

*P*2-*A*1*C*-*A*1. Region 8 is enclosed by the curves *e*, *o*, and *g*. Discontinuous axis-to-cone and continuous cone-to-plane *A*(C*P*) SRT and FOMP-type changes *P*2-*A*1*C*-*A*1 can be observed in systems with initial points inside this region [see Fig. 8(h)]. The anisotropy flow *h*1-*h*2 shown in Fig. 10 indicates that the discontinuous axis-to-cone SRT and the type variation of the FOMP from *P*2 to *A*1*C* are related to the crossing with borderline *o*, and the subsequent continuous cone-to-plane SRT and the *A*1*C*-to *A*1-type variation of the FOMP to the crossing with borderline *l*. The disappearance of the *A*1-type FOMP is due to the crossing of the anisotropy flow with borderline n' at the third critical temperature T_{cr3}. Curve *g* in Fig. 5 has been numerically determined by collecting initial points whose anisotropy flows will pass through the point $t(-2,1)$ which is the common crossing point of borderlines *l* and *m*. Equation (B14) in Appendix B describes curve *g* on the basis of Zener's power law. As shown in Fig. 8(h), Δm_{cr} is discontinuous at $T_{cr1}=T_{s1}$, but continuous at $T_{cr2}=T_{s2}$. h_{cr} shows an anomaly at T_{cr2}.

*P*2-*P*1-*A*1. Region 9 is enclosed by line *b* and curves *r* and *g*. Systems with initial points inside this region exhibit a discontinuous axis-to-plane *AP* SRT and the FOMP-type changes *P*2-*P*1-*A*1 [see Fig. 8(i)]. The normalized critical parameters m_{cr}, Δm_{cr}, and h_{cr} for a *P*1 type of FOMP in the three-constant case can be determined by the following equations, using $H_a=2K_1/M_s$ (Ref. 9):

$$5ym_{cr}^4+4ym_{cr}^3+3(x+y)m_{cr}^2+2(x+y)m_{cr}+x+y+1=0, \tag{15}$$

$$\Delta m_{cr}=1-m_{cr}, \tag{16}$$

$$h_{cr}=|m_{cr}(1+2xm_{cr}^2+3ym_{cr}^4)|. \tag{17}$$

As shown in Fig. 8(i), the first critical temperature T_{cr1} corresponding to the disappearance of a *P*2 type of FOMP and the successive onset of a *P*1 type of FOMP can only be distinguished from the kink in the temperature dependence of Δm_{cr}. No anomaly is observed at T_{cr1} in the thermal curve of h_{cr}. From the anisotropy flow *i*1-*i*2 displayed in Fig. 10, one sees that the type change of the FOMP from *P*2 to *P*1 is due to the crossing of the anisotropy flow with borderline *r*. Subsequently, its crossing with borderline *m* leads to the *AP* SRT and the type variation of FOMP from *P*1 to *A*1 at $T_{cr2}=T_s$. At the borderline *m*, Δm_{cr} is equal to 1 and h_{cr} becomes zero. An *A*1-type FOMP can persist up to the third critical temperature T_{cr3} when the anisotropy flow crosses borderline n'. Above T_{cr2}, Δm_{cr}, (h_{cr}) decreases (increases) monotonically with increasing temperature until T_{cr3}.

*P*1-*A*1. Region 10 is below curve *r* and line *b*, and above line *m*. A discontinuous axis-to-plane *AP* SRT and a change of the FOMP from type *P*1 to *A*1 can be found in the systems with initial points inside this region [see Fig. 9(j)]. The anisotropy flow *j*1-*j*2 shown in Fig. 10 reveals that its crossing with borderline *m* causes the SRT and the type change of the FOMP at T_{cr1}. The FOMP of type *A*1 disappears at T_{cr2} when the anisotropy flow crosses borderline n'. An anomaly can be observed in both the temperature dependence of Δm_{cr} and that of h_{cr} at T_{cr1}.

*P*2-*P*1. Region 11 in Fig. 5 is enclosed by line *b* and curves *r* and *f*. As shown in Fig. 9(k), in the whole temperature range of magnetic order no SRT and only change of the type of FOMP from *P*2 to *P*1 take place. The anisotropy flow *k* shown in Fig. 10 indicates that the type change of the FOMP must be attributed to the crossing with borderline *r*. The subsequent crossing with borderline *n* determines the critical temperature T_{cr2} for the disappearance of a *P*1 type of FOMP. At borderline *n*, Δm_{cr} of a *P*1-type FOMP becomes zero. From 0 K to T_{cr2}, h_{cr} continuously increases to a maximum value. A kink emerges in the temperature dependence of Δm_{cr} at T_{cr1}. If the initial point is on line *b*, a *P*1 type of FOMP can persist up to the Curie temperature, because the anisotropy flow approaches the point $(-\frac{7}{8},0)$ and does not cross the borderline *n*.

*P*1. Region 12 in Fig. 5 is below curve *r* and line *n* and above line *b*. Systems with initial points inside this region exhibit only a *P*1 type of FOMP, and no SRT [see Fig. 9(l)]. When the anisotropy flow *l* in Fig. 10 crosses borderline *n*, the amplitude of the *P*1 type FOMP becomes zero. When the initial point is on line *b*, a *P*1 type of FOMP can be observed in the whole temperature range of magnetic ordering, as the anisotropy flow never crosses borderline *n*.

In the remaining region above curve *q* and line *n*, no FOMP and SRT can be detected at any temperature because the anisotropy flow originating from this region does not cross any borderline for the EMD or the existence of a FOMP in the parameter space (*x*-*y*). The thermal behaviors of FOMP's and SRT's in systems with initial points inside each region in Fig. 5 are summarized in Table 1.

2. $K_1^0<0$

If the sign of K_1^0 is changed, the competition between the anisotropy constants will be varied. Consequently, the phase diagram for the existence of a FOMP is modified. Therefore, different types of thermal behavior of FOMP's and different conditions of their existence are expected in the initial plane x_0-y_0. The phase diagram of the conditions of their existence is shown in detail in Fig. 11, where the lines *l*, *n*, and n' and the curves o', q', and r' are the borderlines between four types of FOMP's: *A*1, *A*1*C*, *A*2, and *P*1*C* at zero temperature. The equations of some borderlines in Fig. 11 are listed in Appendix B. Line *b* starts from the point $s(-\frac{9}{4},\frac{11}{8})$, a common crossing point of the numerically determined curves *c*, c', *j*, and g'. Fourteen types of thermal behavior of FOMP's [(1) *A*1, (2) *A*1*C*-*A*1, (3) *A*1*C*, (4) *A*2-*A*1, (5) *A*2, (6) *P*1*C*-*A*2, (7) *P*1*C*, (8) *P*1*C*-*P*1, (9) *A*2-*P*1*C*-*P*1, (10) *A*2-*P*1, (11) *P*1*C*-*A*2-*P*1, (12) *A*2-*A*1-*P*1-*A*1, (13) *P*1*C*-*A*2-*A*1-*P*1-*A*1, and (14) *P*1*C*-*A*2-*A*1] are found after a systematic investigation of the anisotropy flow of any initial point (x_0, y_0) in the initial parameter space with $K_1^0<0$. For each type of thermal behavior of the FOMP, one representative initial point is se-

TABLE I. Summary of thermal behavior of FOMP's and SRT's observed in a single-ion one-sublattice system with initial point inside each region in Fig. 5 (the case of $K_1^0>0$). The asterisk points to the remaining region outside the 12 nominated regions. The arrows indicate the direction of increasing temperature, and the letter above the arrow denotes the borderline where the transition takes place. The letter between parentheses in the FOMP column is the borderline where the FOMP disappears. The parentheses in the SRT column indicate that the transition is of second order.

No.	FOMP	SRT
1	$A1(n')$	/
2	$A1C \xrightarrow{l} A1(n')$	$(C \xrightarrow{l} P)$
3	$A1C(n')$	$(C \xrightarrow{l} P),/,(C \xrightarrow{K_1=0} A)$
4	$A1C \xrightarrow{o} P2(q)$	$C \xrightarrow{o} A$
5	$P2(q)$	/
6	$P2 \xrightarrow{o} A1C \xrightarrow{o} P2(q)$	$A \xrightarrow{o} C \xrightarrow{o} A$
7	$P2 \xrightarrow{o} A1C(n')$	$A \xrightarrow{o} (C \xrightarrow{l} P),\ A \xrightarrow{o} C,$ $A \xrightarrow{o} (C \xrightarrow{K_1=0} A)$
8	$P2 \xrightarrow{o} A1C \xrightarrow{l} A1(n')$	$A \xrightarrow{o} (C \xrightarrow{l} P)$
9	$P2 \xrightarrow{r} P1 \xrightarrow{m} A1(n')$	$A \xrightarrow{m} P$
10	$P1 \xrightarrow{m} A1(n')$	$A \xrightarrow{m} P$
11	$P2 \xrightarrow{r} P1(n)$	/
12	$P1(n),P1$	/
*	/	/

lected to show the thermal variation of the normalized amplitude and critical field of the FOMP, and the normalized angle of the EMD with respect to the *c* axis (if an SRT exists) in Figs. 12–16. Some relevant anisotropy flows may be found in Fig. 10 by looking for the same notation.

*A*1. The largest region in Fig. 11, region 1, is located above curve r' and line *l*. No SRT and only an *A*1 type of FOMP can be observed in systems with initial points inside this region [Fig. 12 (m)]. The critical temperature T_{cr} for the *A*1 type of FOMP is reached when the anisotropy flow *m* in the bottom part of Fig. 10 crosses the borderline n'. Δm_{cr} decreases, whereas h_{cr} increases with increasing temperature.

*A*1*C*-*A*1. Region 2 in Fig. 11 is below line *l*, and above curve *e*. Systems with initial points inside this region exhibit a continuous cone-to-plane (*CP*) SRT and a FOMP type changes from *A*1*C* to *A*1 [Fig. 12(n)]. The crossing of trajectory *n* in Fig. 10 with the borderline *l* corresponds to this SRT and the change in the type of FOMP. The crossing with borderline n' corresponds to the disappearance of the *A*1-type FOMP at T_{cr2}. A sharp peak in the thermal curve of h_{cr} occurs at the first critical temperature at T_{cr1} $(=T_s)$. Curve *e* is numerically determined by collecting the initial points whose trajectories flow through the crossing point of the borderlines *l* and n'. Equation (B12) in Appendix B describes curve *e* within Zener's power law.

*A*1*C*. Region 3 in Fig. 11 is below the curve *e*. Like region 3 in the case of $K_1^0>0$, line *b* also cuts this region into two subregions. In the region below line *b*, $K_1(t)$ has one zero point and a continuous cone-to-axis (*CA*) SRT can be observed, while, in the region above line *b*, $K_1(t)$ has no zero point and a continuous cone-to-plane (*CP*) SRT exists [Fig. 12(o)]. If the initial point is just on line *b*, no SRT is observed during the whole temperature range of magnetic order. Below the SRT temperature T_s for (*CP*) or (*CA*), the *A*1*C* type of FOMP reaches its critical temperature T_{cr} when the anisotropy flow *o* in Fig. 10 crosses the borderline n'. Above the critical temperature T_{cr} for an *A*1*C* type of FOMP, if the anisotropy flow crosses borderline *l*, (*CP*) SRT occurs; if $K_1(t)$ changes its sign, (*CA*) SRT takes place at the zero point of $K_1(t)$.

*A*2-*A*1. Region 4 in Fig. 11 is below curve r' and above the curves c', o', and *i*. Systems with initial points inside this region exhibit a change of FOMP from *A*2 type to *A*1 type, but no SRT. The normalized critical parameters Δm_{cr} and h_{cr} for an *A*2-type FOMP in the three-constants case can be determined by the following equations using the definition of $H_a=[-2(K_1+2K_2+3K_3)]/M_s$ (Ref. 9):

$$\Delta m_{cr}=\left[\frac{5(x+3y)-G}{6y}\right]^{1/2}, \tag{18}$$

with

$$G=(60y-11x^2+81y^2+54xy)^{1/2},$$

and

$$h_{cr}=\frac{A'}{5}\left[2-\frac{(x+3y)\{17(x+3y)-G\}}{30y(1+2x+3y)}\right], \tag{19}$$

with

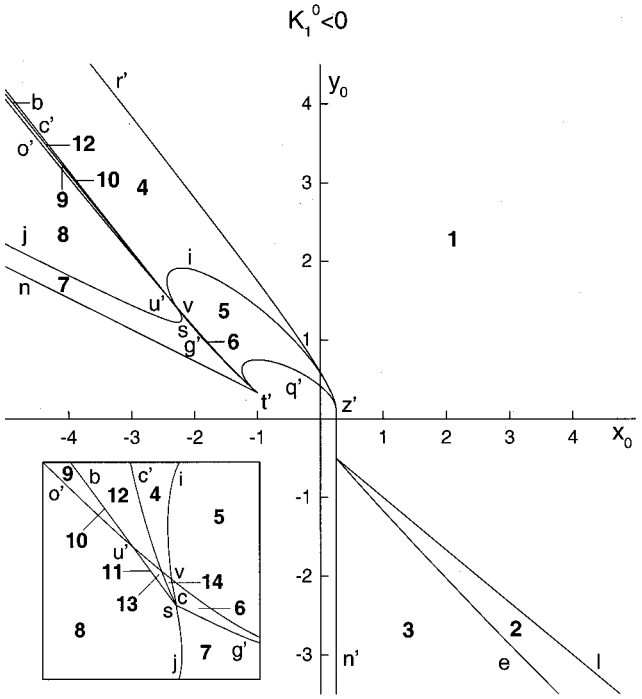

FIG. 11. Phase diagram for different kinds of thermal behavior of the FOMP's in the initial parameter space (x_0-y_0) with $K_1^0<0$: (1) $A1$, (2) $A1C$-$A1$, (3) $A1C$, (4) $A2$-$A1$, (5) $A2$, (6) $P1C$-$A2$, (7) $P1C$, (8) $P1C$-$P1$, (9) $A2$-$P1C$-$P1$, (10) $A2$-$P1$, (11) $P1C$-$A2$-$P1$, (12) $A2$-$A1$-$P1$-$A1$, (13) $P1C$-$A2$-$A1$-$P1$-$A1$, and (14) $P1C$-$A2$-$A1$. The curves r', o', and q' and the straight lines l, n, and n' are the borderlines between four types of FOMP's: $A1$, $A1C$, $A2$, and $P1C$ at zero temperature. The configurations of the different regions around point u' are schematically represented in the inset.

$$A' = \left[\frac{3(x+3y)+G}{10y}\right]^{1/2}.$$

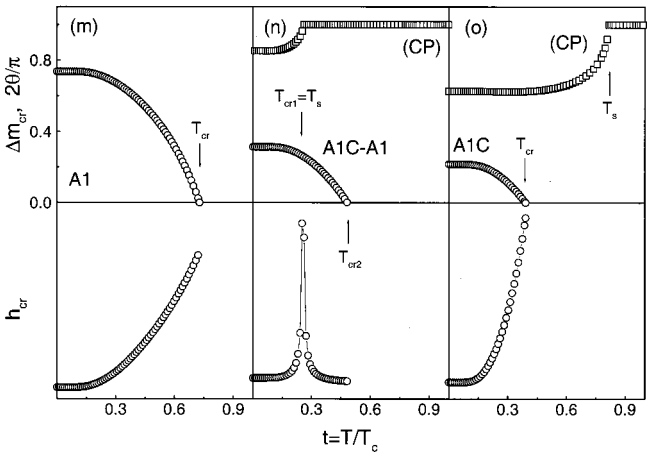

FIG. 12. Temperature variation of the angle of the EMD with respect to the c axis normalized to $\pi/2$ (open squares), the normalized amplitude, and the critical field of FOMP's (open circles) in some typical systems in the case of $K_1^0<0$. The initial parameters used during the calculation are (m) (6.0,7.0), (n) (7.0,−5.3), and (o) (5.0,−5.5).

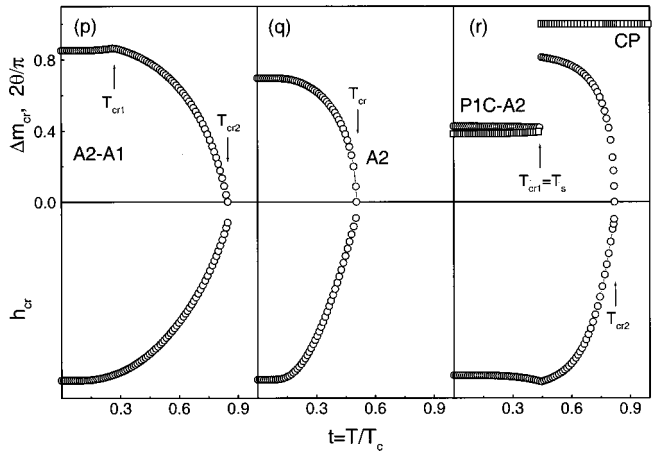

FIG. 13. Temperature variation of the angle of the EMD with respect to the c axis normalized to $\pi/2$ (open square), the normalized amplitude, and the critical field of FOMP's (open circles) in some typical systems in the case of $K_1^0<0$. The initial parameters used during the calculation are (p) (−3.8,3.8), (q) (−2.0,1.5), and (r) (2.2,1.33).

As shown in Fig. 13(p), the first critical temperature T_{cr1}, at which the change takes place from $A2$ to $A1$ types of FOMP, can be seen as a kink in the temperature dependence of Δm_{cr}. However, no anomaly occurs in the temperature dependence of h_{cr} at T_{cr1}. The trajectory p in Fig. 10 suggests that its crossings with borderlines r' and n' correspond with the change of the FOMP from $A2$ to $A1$ type, and with the disappearance of an A1-type FOMP, respectively. Curve i has been numerically determined by collecting the initial points whose anisotropy flows pass through the crossing point $z'(\frac{1}{4},\frac{1}{8})$ of the borderlines r' and n'. Curve i crosses with curves o' and c at point v. With Zener's power law, one can derive Eq. (B16) in Appendix B, that describes curve i.

$A2$. Region 5 in Fig. 11 is below the curve i and above the

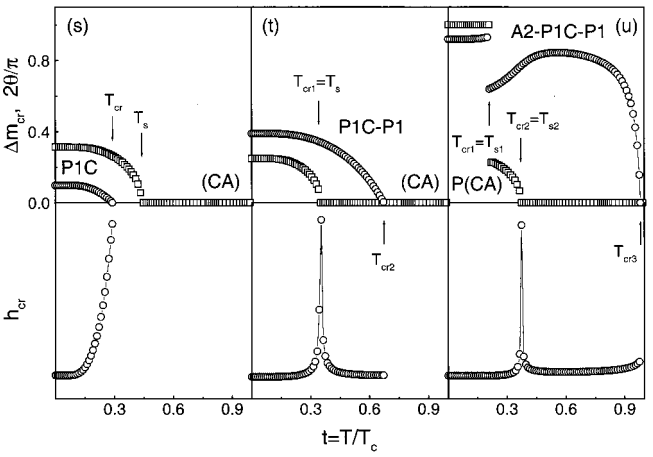

FIG. 14. Temperature variation of the angle of the EMD with respect to the c axis normalized to $\pi/2$ (open square), the normalized amplitude, and the critical field of FOMP's (open circles) in some typical systems in the case of $K_1^0<0$. The initial parameters used during the calculation are (s) (−2.6,1.1), (t) (−4.0,2.5), and (u) (−4.0,3.08).

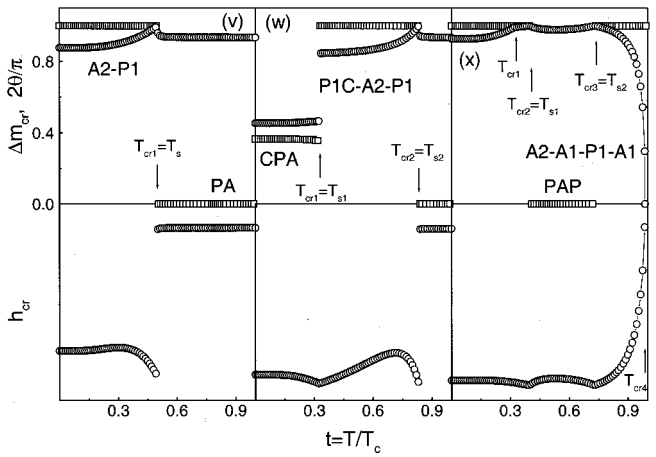

FIG. 15. Temperature variation of the angle of the EMD with respect to the *c* axis normalized to $\pi/2$ (open squares), the normalized amplitude, and the critical field of FOMP's (open circles) in some typical systems in the case of $K_1^0<0$. The initial parameters used during the calculation are (*v*) $(-3.0,2.125)$, (*w*) $(-2.35,1.475)$, and (*x*) $(-5.0,4.16)$.

curves o' and q'. No SRT and only an $A2$ type of FOMP is observed in systems with initial points inside this region. In Fig. 13(q) it can be seen that Δm_{cr} of the FOMP becomes zero while h_{cr} reaches a maximum at the critical temperature T_{cr}. This happens when the trajectory q in Fig. 10 crosses the borderline q'.

$P1C$-$A2$. Region 6 is enclosed by curves c, o', and g'. A discontinuous cone-to-plane *CP* SRT and a change of FOMP from $P1C$ to $A2$ type can be observed in the systems with

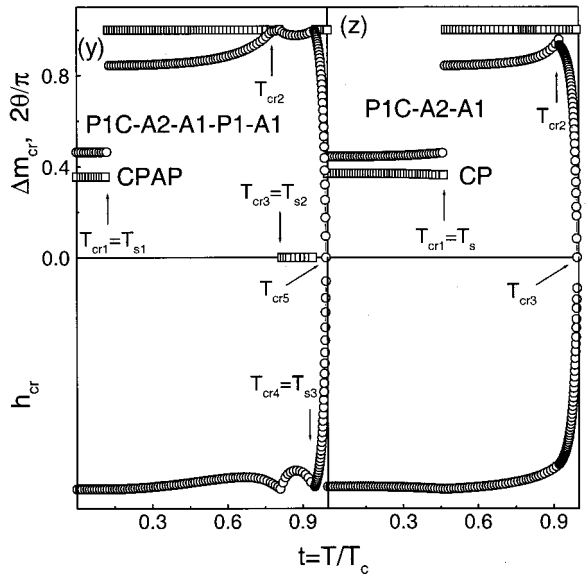

FIG. 16. Temperature variation of the angle of the EMD with respect to the *c* axis normalized to $\pi/2$ (open squares), the normalized amplitude, and the critical field of FOMP's (open circles) in some typical systems in the case of $K_1^0<0$. The initial parameters used during the calculation are (*y*) $(-2.4,1.5253)$ and (*z*) $(-2.3,1.4253)$.

initial points inside this region [Fig. 13(r)]. When trajectory *r* in Fig. 10 crosses borderline o', the SRT and the type change of the FOMP take place at $T_{cr1}=T_s$. Crossing with borderline q' leads to the disappearance of an $A2$-type FOMP at T_{cr2}. Curve *c* is the same as that in Fig. 5, and curve g' has numerically been determined by collecting the initial points whose anisotropy flows pass the crossing point $t'(-1,\frac{1}{3})$ of borderlines o', q', and *n*. Equation (B15) in Appendix B describes curve g' within Zener's power law. Δm_{cr} shows a discontinuous jump at T_{cr1}.

$P1C$. Only a $P1C$-type FOMP exists in systems with an initial point inside region 7 which is below curves *j* and g' and above line *n*. Line *b* separates this region into two subregions. In the region below line *b*, a continuous cone-to-axis (*CA*) SRT can be observed [Fig. 14(s)], while in the region above line *b*, a continuous cone-to-plane (*CP*) SRT exists. If the initial point is just on line *b*, no SRT occurs. Below the SRT temperature for (*CP*) and (*CA*) SRT's, when the anisotropy flow $s1$-$s2$ in Fig. 10 crosses borderline *n*, the $P1C$-type FOMP reaches its critical temperature T_{cr}. Above the critical temperature T_{cr}, if the anisotropy flow crosses borderline *l*, (*CP*) SRT occurs; if $K_1(t)$ changes its sign like the anisotropy flow *s* in Fig. 10, (*CA*) SRT takes place at the zero point of $K_1(t)$. Curve *j* has been numerically determined by collecting the initial points whose critical temperature T_{cr} of the $P1C$-type FOMP is just equal to the transition temperature T_s of the (*CA*) SRT.

$P1C$-$P1$. Region 8 is above curve *j* and below line *b* and curve o'. A continuous cone-to-axis (*CA*) SRT and a change of the FOMP from $P1C$ to $P1$ type exist in systems with initial points inside this region [Fig. 14(t)]. The trajectory $t1$-$t2$ in Fig. 10 shows that the SRT and the type change of the FOMP take place at the zero point of $K_1(t)$, and that the crossing with borderline *n* in the parameter space with $K_1>0$ corresponds with the disappearance of a $P1$-type FOMP. A sharp peak clearly emerges in the temperature dependence of h_{cr} at T_{cr1} $(=T_s)$, since h_{cr} determined by Eq. (17) tends to infinity at the zero point of $K_1(t)$. No anomaly occurs in the temperature dependence of Δm_{cr} when the type of FOMP changes from $P1C$ to $P1$.

$A2$-$P1C$-$P1$. Region 9 is above curve o' and below line *b*. A discontinuous plane-to-cone and a continuous cone-to-axis $P(CA)$ SRT and FOMP-type changes $A2$-$P1C$-$P1$ can be found in the systems with initial points inside this region [Fig. 14(u)]. From the trajectory $u1$-$u2$ in Fig. 10, one knows that the discontinuous plane-to-cone SRT and the type variation of FOMP from $A2$ to $P1C$ are due to the crossing with borderline o'. A discontinuous jump of Δm_{cr} occurs at T_{cr1} $(=T_{s1})$ together with the type variation of the FOMP from $A2$ to $P1C$. The ensuing continuous cone-to-axis SRT and the type change of the FOMP from $P1C$ to $P1$ have the same origin as discussed above in region 8.

$A2$-$P1$, $P1C$-$A2$-$P1$. Both regions 10 and 11 in Fig. 11 are on line *b* that starts from point *s* and crosses curve o' at point u'. The part of line *b* above point u' belongs to region 10, while the part between points u' and *s* belongs to region 11. When the initial point is on line *b* above point *s*, $K_1(t)$ has one zero point; thus its anisotropy flow consists of two

parts. The first one is along line b from the initial point to infinity, and the second one is along line b from infinity in the third quadrant to the point $(-\frac{7}{8},0)$ in the parameter space with $K_1>0$. Therefore, when the initial point is in region 10, the system is expected to have a discontinuous plane-to-axis SRT, and a type change of the FOMP from $A2$ to $P1$ [Fig. 15(v)] occurs at the zero point of $K_1(t)$. If the initial point is in region 11, a discontinuous cone-to-plane SRT and type change of FOMP from $P1C$ to $A2$ will take place [Fig. 15(w)] before the zero point of $K_1(t)$ when the anisotropy flow crosses the borderline o'. In both cases, a $P1$-type FOMP may persist up to the Curie temperature.

$A2$-$A1$-$P1$-$A1$. Region 12 is above line b and curve o' and below curve c'. A discontinuous plane-to-axis and a discontinuous axis-to-plane *PAP* SRT and a change of type of FOMP $A2$-$A1$-$P1$-$A1$ can be observed in systems with initial points inside this region [Fig. 15(x)]. One finds from the trajectory $x1$-$x2$-$x3$ in Fig. 10 that $K_1(t)$ has two zero points. When trajectory $x1$ crosses borderline r', the type of FOMP changes from $A2$ to $A1$. Then, after the first zero point of $K_1(t)$, when trajectory $x2$ crosses borderline m twice, the *PAP* SRT and the type change of the FOMP $A1$-$P1$-$A1$ take place before the second zero point of $K_1(t)$. The curve c' has been numerically determined by collecting the initial points whose anisotropy flows are tangent to the borderline m in the parameter space with $K_1>0$.

$P1C$-$A2$-$A1$-$P1$-$A1$. Region 13 in Fig. 11 is enclosed by line b and the curves o' and c'. With increasing temperature, systems with initial points inside this region exhibit discontinuous cone-to-plane, discontinuous plane-to-axis, and discontinuous axis-to-plane *CPAP* SRT's, together with a type change of the FOMP: $P1C$-$A2$-$A1$-$P1$-$A1$ [Fig. 16(y)]. The discontinuous cone-to-plane SRT and the type change of the FOMP from $P1C$ to $A2$ are connected with the crossing of the anisotropy flow with borderline o', and the successive *PAP* SRT and type change of the FOMP $A2$-$A1$-$P1$-$A1$ are the same as in region 12.

$P1C$-$A2$-$A1$. Region 14 is enclosed by curves c', c, and o'. A discontinuous cone-to-plane *CP* SRT and a change of type of FOMP $P1C$-$A2$-$A1$ are found for systems with initial points inside this region [Fig. 16(z)]. The crossing of the first part of the trajectory $z1$-$z2$-$z3$ in Fig. 10, with borderline o', is connected with SRT and the type change of the FOMP from $P1C$ to $A2$. The subsequent change of FOMP from $A2$ to $A1$ type arises from the crossing with borderline r'. Finally, when the third part of the trajectory $z1$-$z2$-$z3$ crosses borderline n' in the first quadrant, the $A1$-type FOMP reaches its critical temperature T_{cr3}.

In the remaining region below line n and curve q' in Fig. 11, no FOMP can be observed at any temperature because the anisotropy flow originating from this region does not cross any borderline for the existence of a FOMP in the parameter space (x-y). As to SRT, this region can be divided into three subregions by lines l and b (see Fig. 9 in Ref. 22). In the subregion above line l, no SRT can be observed. A continuous cone-to-plane (*CP*) SRT can be observed in the subregion between lines l and b, and a continuous cone-to-axis (*CA*) SRT in the subregion below line b. The thermal behavior of the FOMP's and SRT's existing in systems with initial points inside each region in Fig. 11 are summarized in Table II.

So far, we have analyzed the 12 (Fig. 5) and 14 (Fig. 11) types of thermal behaviors of the FOMP's for the cases of $K_1^0>0$ and $K_1^0<0$, respectively. In total, there are 23 different types of thermal behaviors of the FOMP in a single-ion one-sublattice system, depending on the different combinations of the three initial anisotropy constants. In the case of $K_3^0=0$, only three kinds of thermal behaviors of the FOMP were found. This demonstrates that the third anisotropy constant plays a highly important role in diversifying the temperature behavior of the system. Further inspection reveals that the 23 types of thermal behavior of the FOMP can be regarded as different assemblies of 17 kinds of elementary thermal variations of the FOMP: (1) $A1$, (2) $A1C$, (3) $A2$, (4) $P1$, (5) $P1C$, (6) $P2$, (7) $A2$-$A1$, (8) $P2$-$P1$, (9) $A1C$-$A1$, (10) $A1C$-$P2$, (11) $P2$-$A1C$, (12) $P1$-$A1$, (13) $A1$-$P1$, (14) $P1C$-$A2$, (15) $A2$-$P1C$, (16) $P1C$-$P1$, and (17) $A2$-$P1$. The last arisen FOMP disappears in Fig. 10 at borderline n' for the $A1$ and $A1C$ variations, at q' for the $A2$ variation, at n for the $P1$ and $P1C$ variations, and at q for the $P2$ variation. Type changes $A2$-$A1$ and $P2$-$P1$ of the FOMP occur at borderlines r' and r, respectively. No SRT takes place at the critical temperatures for these two kinds of type changes of the FOMP, and the kink in the thermal curve of Δm_{cr} provides a straightforward method to determine the critical temperatures. The other nine kinds of type changes of the FOMP are accompanied by some kinds of SRT occurring at the critical temperatures. The type change $A1C$-$A1$ of the FOMP occurs at borderline 1 together with (*CP*) SRT, $A1C$-$P2$ at o together with *CA*, $P2$-$A1C$ at o together with *AC*, $P1$-$A1$ at m together with *AP*, $A1$-$P1$ at m together with *PA*, $P1C$-$A2$ at o' together with *CP*, $A2$-$P1C$ at o' together with *PC*, $P1C$-$P1$ at the zero point of $K_1(t)$ together with (*CA*), $A2$-$P1$ at the zero point of $K_1(t)$ together with *PA*. In these nine types of changes of the FOMP, the critical temperature of the FOMP is equal to the SRT temperature.

IV. SUMMARY

We have systematically investigated all possible types of the thermal behavior of the FOMP in a single-ion one-sublattice system within the two- and three-constant approximations to the uniaxial anisotropy free energy. Based on the relations between the anisotropy constants and the anisotropy coefficients, we have employed a powerful parameter method to calculate the temperature behavior of a system within the MF approximation. An analysis of the anisotropy flow in the parameter space has enabled us to find all possible types of thermal variations of the FOMP. In the two-constant approximation, there are three types of thermal behaviors of the FOMP. In the three-constant approximation, 12 types are found in the case of $K_1^0>0$ and 14 types in the case of $K_1^0<0$. The phase diagrams concerning the conditions for their existence in the initial parameter spaces are presented after exhausting the observation of the anisotropy flows originating from different initial points. The relation

TABLE II. Summary of the thermal behavior of FOMP's and SRT's observed in a single-ion one-sublattice system with an initial point inside each region in Fig. 11 (in the case of $K_1^0<0$). The asterisk points to the remaining region outside the 14 nominated regions. The arrow indicates the direction of increasing temperature, and the letter above it is the borderline where the transition takes place. The letter inside the parentheses in the FOMP column is the borderline where the FOMP disappears. The parentheses in the SRT column indicate that the transition is of second order.

No.	FOMP	SRT
1	$A1(n')$	/
2	$A1C \xrightarrow{l} A1(n')$	$(C \xrightarrow{l} P)$
3	$A1C(n')$	$(C \xrightarrow{K_1=0} A),/,(C \xrightarrow{l} P)$
4	$A2 \xrightarrow{r'} A1(n')$	/
5	$A2(q')$	/
6	$P1C \xrightarrow{o'} A2(q')$	$C \xrightarrow{o'} P$
7	$P1C(n)$	$(C \xrightarrow{K_1=0} A),/,(C \xrightarrow{l} P)$
8	$P1C \xrightarrow{K_1=0} P1(n)$	$(C \xrightarrow{K_1=0} A)$
9	$A2 \xrightarrow{o'} P1C \xrightarrow{K_1=0} P1(n)$	$P \xrightarrow{o'} (C \xrightarrow{K_1=0} A)$
10	$A2 \xrightarrow{K_1=0} P1$	$P \xrightarrow{K_1=0} A$
11	$P1C \xrightarrow{o'} A2 \xrightarrow{K_1=0} P1$	$C \xrightarrow{o'} P \xrightarrow{K_1=0} A$
12	$A2 \xrightarrow{r'} A1 \xrightarrow{m} P1 \xrightarrow{m} A1(n')$	$P \xrightarrow{m} A \xrightarrow{m} P$
13	$P1C \xrightarrow{o'} A2 \xrightarrow{r'} A1 \xrightarrow{m} P1 \xrightarrow{m} A1(n')$	$C \xrightarrow{o'} P \xrightarrow{m} A \xrightarrow{m} P$
14	$P1C \xrightarrow{o'} A2 \xrightarrow{r'} A1(n')$	$C \xrightarrow{o'} P$
*	/	$(C \xrightarrow{K_1=0} A),/,(C \xrightarrow{l} P)$

between the SRT's and the thermal behavior of FOMP's has been discussed in detail. Seventeen types of elementary thermal changes of the FOMP's have been derived from all the possible types of thermal behavior of the FOMP's. The normalized amplitude of the FOMP's, the critical field, and the critical temperature are given for each type of change and/or disappearance of the FOMP's. Prototype substances to which our analysis applies are all materials in which there is a well-defined single-ion contribution to the overall anisotropy arising from magnetic rare-earth ions.

ACKNOWLEDGMENTS

The present work was carried out within the scientific exchange program between China and the Netherlands, and partly supported by the National Natural Science Foundation of China (Grant No. 59725103) and by the Science and Technology Commission of Shenyang and Liaoning.

APPENDIX A

In uniaxial symmetry, the relations between the anisotropy constants K_i and anisotropy coefficients $\overline{\kappa_n}$ are

$$K_1(t)=(K_1^0+\tfrac{8}{7}K_2^0+\tfrac{8}{7}K_3^0)\overline{\kappa_2}(t) - \tfrac{8}{7}(K_2^0+\tfrac{18}{11}K_3^0)\overline{\kappa_4}(t)+\tfrac{8}{11}K_3^0\overline{\kappa_6}(t), \quad \text{(A1)}$$

$$K_2(t)=(K_2^0+\tfrac{18}{11}K_3^0)\overline{\kappa_4}(t)-\tfrac{18}{11}K_3^0\overline{\kappa_6}(t), \quad \text{(A2)}$$

$$K_3(t)=K_3^0\overline{\kappa_6}(t). \quad \text{(A3)}$$

The anisotropy coefficients $\overline{\kappa_n}$ can be expressed as linear combination of the moments $M_n \equiv \langle(\hat{J}_z)^n\rangle$:

$$\overline{\kappa_2}=\frac{1}{p_2(J)}[3M_2-J(J+1)], \quad \text{(A4)}$$

$$\overline{\kappa_4}=\frac{1}{p_4(J)}[35M_4+(25-30J-30J^2)M_2+3J^2(J+1)^2 - 6J(J+1)], \quad \text{(A5)}$$

$$\overline{\kappa_6}=\frac{1}{p_6(J)}\{231M_6+[735-315J(J+1)]M_4+[294 - 525J(J+1)+105J^2(J+1)^2]M_2-60J(J+1) + 40J^2(J+1)^2-5J^3(J+1)^3\}. \quad \text{(A6)}$$

The moments M_n can be deduced from the moment-generating function $\Omega(\alpha,x)$:

$$M_n(x)=\frac{\partial^n}{\partial\alpha^n}\Omega(\alpha,x)\bigg|_{\alpha=0}$$
$$=\frac{\partial^n}{\partial\alpha^n}\frac{\sinh\left[\frac{2J+1}{2}(\alpha+x)\right]\Big/\sinh[(\alpha+x)/2]}{\sinh\left(\frac{2J+1}{2}x\right)\Big/\sinh(x/2)}. \tag{A7}$$

Within the MF approximation, the relation between the generalized effective field x and the normalized temperature t is

$$x=\frac{3}{J+1}\frac{m}{t}. \tag{A8}$$

APPENDIX B

The equations of some borderlines in Figs. 5 and 11 are as follows:[22]

$$l:\quad 2x_0+3y_0+1=0, \tag{B1}$$
$$m:\quad x_0+y_0+1=0, \tag{B2}$$
$$n:\quad 6x_0+15y_0+1=0, \tag{B3}$$
$$n':\quad 4x_0-1=0, \tag{B4}$$
$$o:\quad x_0^2-4y_0=0, \tag{B5}$$
$$o':\quad x_0^2-2x_0y_0-3y_0^2-4y_0=0, \tag{B6}$$
$$q:\quad 3x_0^2-5y_0=0, \tag{B7}$$
$$q':\quad 3x_0^2+8x_0y_0+12y_0^2-5y_0=0, \tag{B8}$$
$$r:\quad x_0^4-5x_0^3y_0+61x_0^2y_0^2+255x_0y_0^3+225y_0^4-8x_0^2y_0+52x_0y_0^2+105y_0^3+16y_0^2=0, \tag{B9}$$
$$r':\quad x_0^4+x_0^3y_0-8x_0^2y_0-36x_0y_0^2-27y_0^3+16y_0^2=0, \tag{B10}$$
$$b:\quad 7x_0+7y_0+8=0, \tag{B11}$$
$$e:\quad 5^{25}y_0^7(7+8x_0+8y_0)^{11}+2^{29}(11x_0+18y_0)^{18}=0, \tag{B12}$$
$$f:\quad 37^{18}y_0^7(7+8x_0+8y_0)^{11}-73^{11}(11x_0+18y_0)^{18}=0, \tag{B13}$$
$$g:\quad 4^{18}y_0^7(7+8x_0+8y_0)^{11}+(11x_0+18y_0)^{18}=0, \tag{B14}$$
$$g':\quad 3^{11}15^7y_0^7(7+8x_0+8y_0)^{11}-(11x_0+18y_0)^{18}=0, \tag{B15}$$
$$i:\quad 8(10y_0)^7(7+8x_0+8y_0)^{11}-(11x_0+18y_0)^{18}=0. \tag{B16}$$

APPENDIX C

The equations of the borderlines among the six types of FOMP's, $A1$, $A1C$, $A2$, $P1$, $P1C$, and $P2$ at arbitrary temperature in Fig. 10 are as follows:[9]

$$l:\quad 2x+3y+1=0, \tag{C1}$$
$$m:\quad x+y+1=0, \tag{C2}$$
$$n:\quad 6x+15y+1=0, \tag{C3}$$
$$n':\quad 4x-1=0, \tag{C4}$$
$$o:\quad x^2-4y=0, \tag{C5}$$
$$o':\quad x^2-2xy-4y-3y^2=0, \tag{C6}$$
$$p:\quad x^2-3y=0, \tag{C7}$$
$$q:\quad 3x^2-5y=0, \tag{C8}$$
$$q':\quad 3x^2+8xy+12y^2-5y=0, \tag{C9}$$
$$r:\quad x^4-5x^3y+61x^2y^2+255xy^3+225y^4-8x^2y+52xy^2+105y^3+16y^2=0, \tag{C10}$$
$$r':\quad x^4+x^3y-8x^2y-36xy^2-27y^3+16y^2=0, \tag{C11}$$

[1] G. Asti, in *Ferromagnetic Materials*, edited by K. H. J. Buschow and E. P. Wohlfarth (Elsevier, Amsterdam, 1990), Vol. 5, pp. 398–464.

[2] M. Yamada, H. Kato, H. Yamamoto, and Y. Nakagawa, Phys. Rev. B **38**, 620 (1988).

[3] T. S. Zhao, H. M. Jin, G. H. Guo, X. F. Han, and H. Chen, Phys. Rev. B **43**, 8593 (1991).

[4] H. M. Jin and Y. Yan, Phys. Rev. B **48**, 1022 (1993).

[5] X. C. Kou, T. S. Zhao, R. Grössinger, H. R. Kirchmayr, X. Li, and F. R. de Boer, Phys. Rev. B **47**, 3231 (1993).

[6] L. Pareti, A. Paoluzi, F. Alberini, M. R. Ibarra, L. Morellon, and P. A. Algarabel, J. Appl. Phys. **76**, 7473 (1994).

[7] P. J. von Ranke, V. K. Pecharsky, K. A. Gschneidner, Jr., and B. J. Korte, Phys. Rev. B **58**, 14 436 (1998).

[8] A. S. Ermolenko and A. F. Rozhda, IEEE Trans. Magn. **MAG-14**, 676 (1978).

[9] G. Asti and F. Bolzoni, J. Magn. Magn. Mater. **20**, 29 (1980).

[10] G. Asti and F. Bolzoni, J. Appl. Phys. **58**, 1924 (1985).

[11] Y. Millev and M. Fähnle, J. Magn. Magn. Mater. **135**, 285 (1994).

[12] Y. Millev and M. Fähnle, Phys. Rev. B **51**, 2937 (1995).

[13] K. H. W. Stevens, in *Magnetism*, edited by G. Rado and H. Suhl (Academic, London, 1963), Vol. 1, pp. 1–24.

[14] M. T. Hutchings, in *Solid State Physics*, edited by F. Seitz and D. Turnbull (Academic, New York, 1964), Vol. 16, pp. 227–275.
[15] C. Zener, Phys. Rev. **96**, 1335 (1954).
[16] F. Keffer, Phys. Rev. **100**, 1692 (1955).
[17] H. B. Callen and E. Callen, J. Phys. Chem. Solids **27**, 1271 (1966).
[18] Y. Millev and M. Fähnle, J. Phys.: Condens. Matter **7**, 6909 (1995).
[19] Y. Millev and M. Fähnle, J. Magn. Magn. Mater. **163**, L264 (1996).
[20] Y. Millev and M. Fähnle, Phys. Rev. B **52**, 4336 (1995).
[21] Y. Millev and M. Fähnle, IEEE Trans. Magn. **MAG-32**, 4743 (1996).
[22] M. H. Yu and Z. D. Zhang, Phys. Rev. B **60**, 12 107 (1999).
[23] K. H. J. Buschow, Rep. Prog. Phys. **54**, 1123 (1991).
[24] E. Callen and H. B. Callen, Phys. Rev. **139**, A455 (1965).
[25] M. I. Darby and E. D. Isaac, IEEE Trans. Magn. **MAG-10**, 259 (1974).
[26] J. Jensen and A. R. Mackintosh, *Rare Earth Magnetism: Structures and Excitations* (Clarendon, Oxford, 1991).
[27] H. Callen and S. Shtrikman, Solid State Commun. **3**, 5 (1965).